MEASUREMENT OF BEHAVIOR OF GAS BUBBLES AND GAS HOLDUP IN A SLURRY BUBBLE COLUMN BY A DUAL ELECTRORESISTIVITY PROBE METHOD

AKIRA YASUNISHI, MIKI FUKUMA AND KATSUHIKO MUROYAMA
Department of Environmental Chemistry and Technology, Tottori University, Tottori 680

Key Words: Chemical Reactor, Slurry Bubble Column, Bubble Column, Bubble Length Distribution, Bubble Velocity Distribution, Gas Holdup

Bubble properties such as gas holdup, bubble frequency, bubble length and bubble rising velocity in a slurry bubble column were measured by using a dual electroresistivity probe method.

The radial distribution of local gas holdup, ε_g, was parabolic in the range, where mean solid holdup, $\bar{\varepsilon}_s$, was less than 0.2. In the range of $\bar{\varepsilon}_s \geq 0.2$, however, ε_g in the region of dimensionless radius, r/R_w, from 0.4 to 0.8 decreased considerably owing to the concentration of bubbles in the central region of the column. The value of cross-sectionally averaged gas holdup, $\bar{\varepsilon}_g$, agreed fairly well with that predicted by Koide's equation for heterogeneous flow in a slurry bubble column.

The cumulative bubble length distribution, F_l, followed a log-normal distribution. On the other hand, the cumulative bubble rising velocity distribution, F_v, followed a normal distribution. The superficial gas velocity, U_g, had little effect on F_l and F_v in the slurry bubble column with high solid content.

When U_g was larger than about 4 cm/s, the median of F_l and that of F_v in the slurry bubble column were larger than the corresponding values in the bubble column. On the other hand, the variance of F_l in the slurry bubble column was almost the same as that in the bubble column and the variance of F_v in the slurry bubble column was smaller than that in the bubble column.

Introduction

Slurry bubble columns are widely used as chemical reactors for various processes in industrial practice. Many research works have been conducted on hydrodynamic characteristics including axial distribution of suspended solids,[2,8,12,17,18] gas holdup[3,8,11,12] and liquid mixing[6,8] and gas-liquid mass transfer[7,9,11] in slurry bubble columns. Recently, the authors[23] have investigated the effect of solid concentration on the volumetric liquid-phase mass transfer coefficient, k_la, and on the axial distribution of solid holdup in the slurry bubble column with a gas-liquid concurrent upflow system.

Bubble properties such as bubble size, bubble rising velocity and gas holdup are very important in analyzing hydrodynamics and gas-liquid mass transfer in the slurry bubble column. A limited amount of data, however, has been presented concerning the bubble diameter[9,12] in the slurry bubble column.

The purpose of this work is to investigate the fundamental properties of gas bubbles such as gas holdup, bubble frequency, bubble size distribution and bubble rising velocity distribution in the slurry bubble column. The bubble properties were measured by using a dual electroresistivity probe method.[4,5,10,13-16,19,21,22]

Received February 5, 1986. Correspondence concerning this article should be addressed to A. Yasunishi.

1. Experimental

1.1 Experimental apparatus

Figure 1 is a schematic diagram of the experimental apparatus. The main experimental column, made of transparent acrylic resin, was 0.15 m in inner diameter and 1.2, 1.7 or 3.2 m in height. Its bottom section was equipped with a bed support made of two sheets of stainless steel wire nets (200 over 12 mesh), a gas distributor and a conical calming section filled with 4-mm Raschig rings. The gas distributor consisted of eight stainless steel tubes of 3 mm O.D. and 2.6 mm I.D. Each of the tubes was equidistantly arranged and horizontally inserted through the column wall toward the axis, protruding 25 mm from the inside wall surface. At the top of the column a cylindrical screen with a diameter of 0.2 m and a height of 0.25 m, made of 200 mesh stainless steel wire net, was installed to prevent particle carryover and to maintain a constant bed height.

Several pairs of stainless steel sheets (25 × 100 mm) were attached to the inside wall surface as electroconductivity probes in the axial direction. The distance between adjacent probes was 0.1 to 0.3 m. Pressure taps were installed along the wall and con-

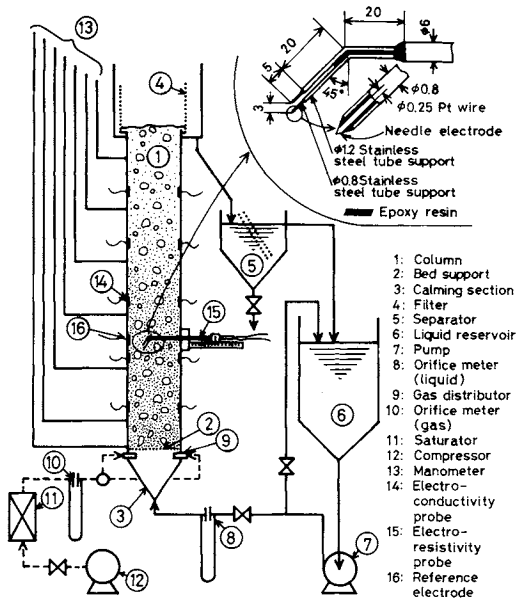

Fig. 1. Schematic diagram of experimental apparatus.

nected to pressure manometers. The distance between adjacent taps was 0.1 to 0.2 m.

A dual electroresistivity probe designed to be movable in the radial direction was installed at a position 0.56 m above the bed support screen. As shown in Fig. 1, the probe was made of 0.25 mm-diameter platinum wire coated with epoxy resin and encased in an 0.8 mm-diameter stainless steel tube except for the sharply finished tip. The front part of the supporting tube was bent by 0.25π rad downward. The vertical distance between the two needle points was 3 mm. A reference electrode, made of stainless steel sheet (25×100 mm), was attached to the inside wall surface facing the probe points.

Water and aqueous solutions of glycerol were used as the liquids. The liquid temperature was maintained at 293.2 K in the liquid reservoir. Air was used as the gas. Glass beads with a density of 2500 $kg \cdot m^{-3}$ were used as the solids. The physical properties of the liquids are presented in **Table 1**. In this case, KCl was added to the liquid, and its concentration was maintained in the range from 5 to 10 $mol \cdot m^{-3}$. The particles properties and the corresponding experimental conditions are presented in **Table 2**.

The axial distribution of solid holdup, ε_s, and the corresponding mean solid holdup, $\bar{\varepsilon}_s$, in the column were preliminarily measured by combining the electroconductivity probe method and the static pressure method.[23] When two slurry layers, i.e. the dense region and the lean region, were formed, the gas holdup and the bubble properties in the dense region were measured by the dual-probe method.

1.2 Method of measuring bubble properties

The electric circuits for the signal processing system are shown in **Fig. 2**. AC voltage at a frequency of

Table 1. Properties of liquids used (at 293.2 K)

Liquid	ρ_l [kg/m^3]	μ_l [mPa·s]	γ_l [mN/m]
Water	998	1.00	72.8
5GL	1012	1.20	72.4
16GL	1040	1.70	71.5
20GL	1051	1.95	71.2
50GL	1127	6.60	68.8

5GL, 16GL, 20GL and 50GL: 5, 16, 20 and 50 vol% glycerol aqueous solution.

Table 2. Particle properties of glass beads and experimental conditions

d_p [mm]	Mesh size [mesh]	Liquid	V_t [cm/s]	H [m]	$\bar{\varepsilon}_s$ [—]
0.056	200–400	Water	0.26	1.2	≤0.4
0.16	80–100	Water	1.63	1.2, 1.7	≤0.4
		5GL	1.42	1.2	≤0.13
		16GL	1.07	1.2	≤0.13
		20GL	0.94	1.2	≤0.13
		50GL	0.29	1.2	≤0.2
0.23	60– 65	Water	2.8	1.7	≤0.4
0.46	32– 35	Water	6.7	3.2	≤0.5

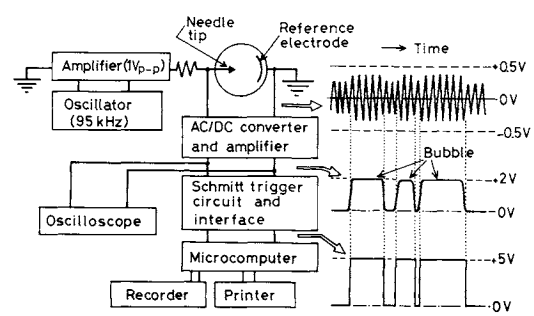

Fig. 2. Electric circuits for electroresistivity probe.

95 kHz was applied to the probe. The difference in conductivities of gas phase and slurry phase was detected by the probe. The output signal from the probe was transformed into a square wave in the wave-reforming section, and finally the reformed signals were processed with a microcomputer (AIM 65, Rockwell International). In the Schmitt trigger circuit, the threshold level of the leading edge of the signal and that of the trailing edge were set at 20% and 15%, respectively, of the highest level of the bubble signal.[4,13,16]

The local gas holdup, ε_g, was determined from the lower probe signal passage as the ratio of the sum of the duration time for the bubble to the measuring period. The local bubble frequency, n_b, was determined from the number of leading edges of the bubble signals. For 89 s, the microcomputer took the data of the signal at 85 μs intervals. After several data processings, the mean values of ε_g and n_b were obtained as

local values in the column. The measurements were carried out at radial positions of 0, 34, 47, 58 and 67 mm from the column axis, which divided the column into 5 annular sections of equal area. The cross-sectionally averaged value of gas holdup, $\bar{\varepsilon}_g$, was obtained from Eq. (1):

$$\bar{\varepsilon}_g=\frac{2}{R_w^2}\int_0^{R_w}\varepsilon_g r dr \tag{1}$$

The cross-sectionally averaged value of bubble frequency, $\bar{n}_b$, was obtained in the same way as that for $\bar{\varepsilon}_g$.

As shown in **Fig.3**, the velocity of a bubble, U_b, and the vertical length (chord length) of the bubble, L_b, were calculated from the lag time between the two signals, Δt, and the duration time for the bubble, τ, respectively:

$$U_b=2l/(\Delta t_1+\Delta t_2) \tag{2}$$

$$L_b=U_b(\tau_1+\tau_2)/2 \tag{3}$$

where l was the distance between two probes and t was the real time.

For the measurements of U_b and L_b, signal acquisition was made by using the microcomputer. For about 3 s, the microcomputer stored the data for the two points simultaneously at 86 μs intervals. The values of Δt_1, Δt_2, τ_1 and τ_2 were then printed out successively, or the stored data were converted to analog signals which were drawn out on a strip chart. From these records, several sets of bubble signals which satisfied all the constraints described below were obtained. The constraints to avoid accounting of unreasonable signal pairs were:

(i) Δt_1 and Δt_2 have the same sign.

(ii) $0.75\leq 2\tau_1/(\tau_1+\tau_2)\leq 1.25$

(iii) The value of U_b calculated from Eq. (2) lies in the range from -0.8 to $+2.5$ m/s.

Note that about 50% of the signal pairs detected by the probe were excluded.

Radial positions for measuring L_b and U_b were 0, 47 and 67 mm from the column axis. All the effective data obtained at these three measuring positions were summed up to get the cross-sectionally averaged bubble properties. Although the bubble frequency decreased appreciably with radial distance from the axis, the signal processing time at each measuring position was almost equal. The total number of effective bubbles was 50 to 120 for each run.

2. Results and Discussion

2.1 Gas holdup and bubble frequency

Figure 4 shows typical radial distributions of local gas holdup, ε_g, and those of bubble frequency, n_b, for various superficial gas velocities, U_g, in the slurry bubble column. The value of ε_g takes on a maximum

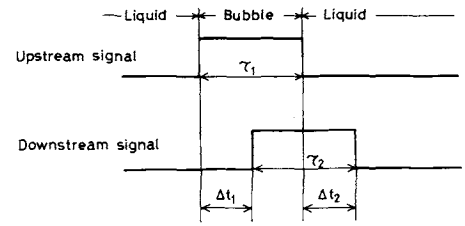

Fig. 3. Relationship between probe signals for the two probes.

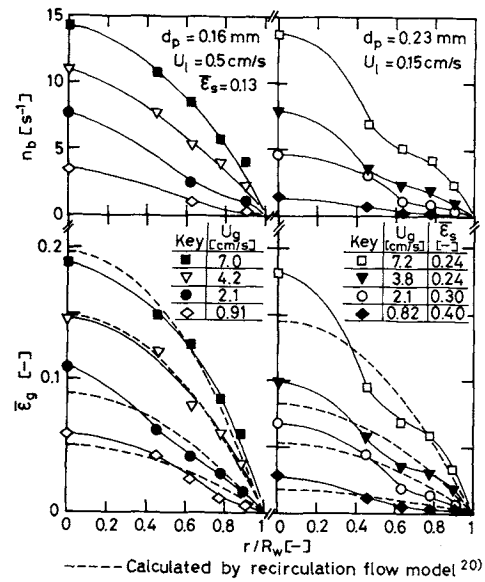

Fig. 4. Radial distributions of gas holdup and bubble frequency in a slurry bubble column.

at the axis and decreases with increasing radial distance, approaching zero at the wall. The radial distribution of ε_g can be expressed well by the parabolic profile from the recirculation flow model[20] for the range of $\bar{\varepsilon}_s<0.2$. In the range of $\bar{\varepsilon}_s\geq 0.2$, the value of ε_g in the region of r/R_w from 0.4 to 0.8 decreases considerably. The shape of radial distribution of n_b resembles that of ε_g for the corresponding condition.

Figure 5 shows the relationships between the cross-sectionally averaged gas holdup, $\bar{\varepsilon}_g$, and U_g in the slurry bubble column for various particle diameters and $\bar{\varepsilon}_s$. The value of $\bar{\varepsilon}_g$ increases with increasing U_g and decreases with increasing $\bar{\varepsilon}_s$. The estimated values of $\bar{\varepsilon}_g$ from the correlation equation of Akita and Yoshida[1] for the bubble column and those from Koide's equation[11] for heterogeneous flow in a slurry bubble column are shown in the figure. The values of $\bar{\varepsilon}_g$ observed agree with those estimated by these correlations for the corresponding operational conditions.

The values of $\bar{\varepsilon}_g$ in the glass beads-water slurry observed by Kojima and Asano[12] and those in the glass beads-sodium sulfite aqueous solution slurry observed by Kato *et al.*[9] are also shown in the figure. The value of $\bar{\varepsilon}_g$ of Kojima and Asano is larger than that in this work at high U_g. This deviation may be

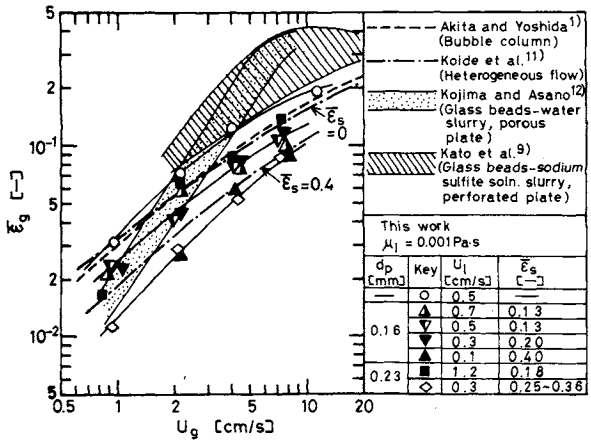

Fig. 5. Effects of $\bar{\varepsilon}_s$ and d_p on $\bar{\varepsilon}_g$ in a slurry bubble column.

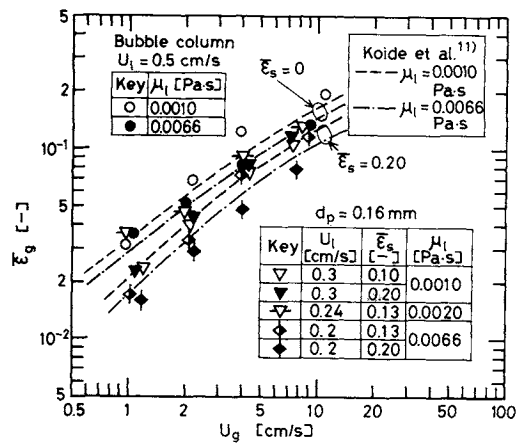

Fig. 6. Effect of μ_l on $\bar{\varepsilon}_g$ in a slurry bubble column.

due to the difference in type of gas distributor. The value of $\bar{\varepsilon}_g$ of Kato *et al.* is much larger than that in this work. However, the effect of $\bar{\varepsilon}_s$ on $\bar{\varepsilon}_g$ is similar to that observed in this work.

Figure 6 shows that the effect of μ_1 on $\bar{\varepsilon}_g$ is small in the slurry bubble column in the range of $\bar{\varepsilon}_s \leq 0.13$. However, at $\bar{\varepsilon}_s = 0.20$, $\bar{\varepsilon}_g$ decreases gradually with increasing μ_1. The values of $\bar{\varepsilon}_g$ estimated by Koide's equation[11] agree with those observed in this work.

Kara *et al.*[6] reported that $\bar{\varepsilon}_g$ in a coal–water slurry decreased with increasing $\bar{\varepsilon}_s$. The values of $\bar{\varepsilon}_g$ in the column with 0.07 mm coal particles observed by Kara *et al.* agree fairly well with those for small particles in this work.

Figure 7 shows that the observed values of $\bar{\varepsilon}_g$ at a small $\bar{\varepsilon}_s$ in the slurry bubble column and those in the bubble column are slightly larger than those predicted by Koide's equation.[11] However, the observed values in this work agree fairly well with those predicted with a coefficient of variation of 28%. From the above results, it may be remarked that Koide's equation is applicable to the slurry bubble column with high solid content up to $\bar{\varepsilon}_s = 0.4$.

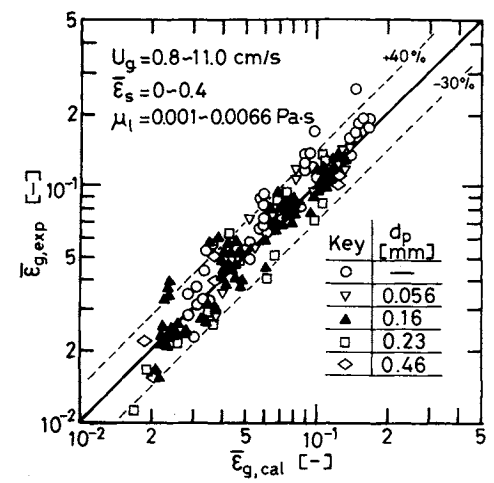

Fig. 7. Comparison of $\bar{\varepsilon}_g$ values estimated by Koide's equation with those observed.

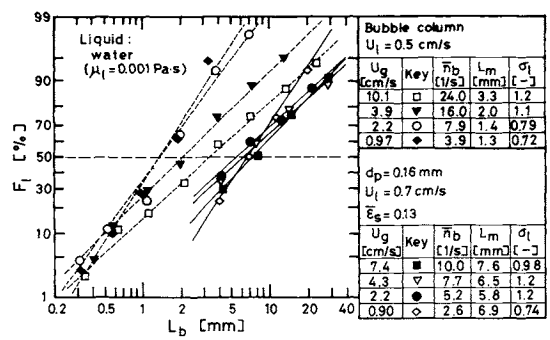

Fig. 8. Cumulative bubble length distribution in a bubble column and a slurry bubble column.

2.2 Distributions of bubble properties

Figure 8 shows the cumulative bubble length distributions, F_l, in the bubble column and those in the slurry bubble column. The values of $\bar{n}_b$ are also noted in the figure. The bubble length distribution for both the bubble column and the slurry bubble column follows a log-normal distribution. This trend is similar to that observed by Akita and Yoshida[1] in the bubble column. The values of median, L_m, and logarithmic standard deviation, σ_l, for F_l are also noted in the figure.

In the bubble column, most of the values of L_b are less than 5 mm and the value of σ_l is small in the range of $U_g \leq 2.2$ cm/s, where the flow mode is termed homogeneous flow (Deckwer *et al.*[3]). In the range of $U_g \geq 3.9$ cm/s, where the flow mode is termed heterogeneous flow (Deckwer *et al.*[3]), large bubbles of $L_b \geq 10$ mm are produced and the values of L_m and σ_l increase with U_g.

In the slurry bubble column at $\bar{\varepsilon}_s = 0.13$, large bubbles appear even at small U_g. U_g has little effect on F_l except in the region of U_g less than about 1 cm/s. The value of σ_l for the slurry bubble column is similar in magnitude to that for heterogeneous flow in the bubble column, while the value of L_m for the former is two or three times as large as that for the latter. The value of $\bar{n}_b$ for the slurry bubble column is much

smaller than that for the bubble column at the same U_g.

Figure 9 shows the cumulative bubble velocity distributions, F_v, in the bubble column and those in the slurry bubble column. The experimental conditions in this figure are consistent with those in Fig. 8. The bubble velocity distribution in both the bubble column and the slurry bubble column follows a normal distribution. The values of median, U_m, and the standard deviation, σ_v, for F_v are also noted in the figure.

In the range of $U_g \leq 2.2$ cm/s for the bubble column, the value of σ_v is small and the values of U_b mostly lie in the range from -0.4 to 0.6 m/s. On the other hand, in the range of $U_g \geq 3.9$ cm/s the distribution extends to both directions of the U_b coordinate. The value of σ_v increases with U_g, but that of U_m remains almost constant.

No appreciable effect of U_g on the bubble velocity distribution is resulted from changing U_g from 0.8 to 8 cm/s in the slurry bubble column. The values of U_b mostly lie in the range from 0 to 1.4 m/s. The ratio of the numbers of descending bubbles to the total for the slurry bubble column is much smaller than that for heterogeneous flow in the bubble column. The value of U_m for the slurry bubble column is about three times as large as that for heterogeneous flow in the bubble column, while the value of σ_v for the former is smaller than that for the latter.

From Figs. 8 and 9, it may be considered that the growth of a bubble in a slurry bubble column may be enhanced by the increased interaction between bubble surface and slurry particles. Thus, in the slurry bubble column with high solid content the bubbles grow rapidly just above the gas distributor even at small U_g. The small bubbles in the slurry bubble column rise with relatively high speed following the large bubbles.

Conclusions

The following results are obtained for the bubble properties in a slurry bubble column.

1) The shape of the radial distributions of local gas holdup and bubble frequency is parabolic in the range of mean solid holdup, $\bar{\varepsilon}_s$, less than 0.2. In the range of $\bar{\varepsilon}_s \geq 0.2$ the gas holdup and the bubble frequency decrease considerably in the region of r/R_w from 0.4 to 0.8.

2) The cross-sectionally averaged gas holdup, $\bar{\varepsilon}_g$, decreases with increasing $\bar{\varepsilon}_s$, but the effect of liquid viscosity on $\bar{\varepsilon}_g$ is not appreciable. In the range of $\bar{\varepsilon}_s \leq 0.4$, $\bar{\varepsilon}_g$ can be predicted fairly well by Koide's equation for heterogeneous flow.

3) The cumulative bubble length distribution, F_l, follows a log-normal distribution. F_l in the slurry bubble column with high solid content lies in a larger bubble size region than that for heterogeneous flow in bubble column, and is little affected by the gas velocity.

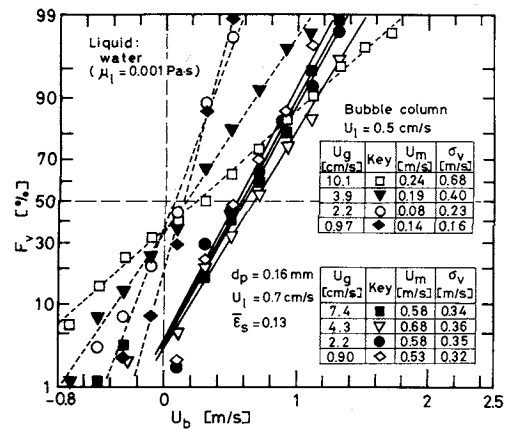

Fig. 9. Cumulative bubble velocity distribution in a bubble column and a slurry bubble column.

4) The cumulative bubble velocity distribution, F_v, follows a normal distribution. F_v in the slurry bubble column with high solid content lies in a larger velocity region than that in the bubble column, and is little affected by the gas velocity.

Acknowledgment

The authors are grateful to Mr. T. Matsuoka (Dept. of Electrical Engineering, Tottori University) and Mr. M. Shigemoto for their participation in our manufacture of a computer-controlled data acquisition system, and express appreciation to Mr. A. Mōri, Mr. Y. Kodera and Mr. T. Ishitobi for their experimental assistance.

Nomenclature

d_p	=	particle diameter	[mm]
F_l	=	cumulative bubble length distribution	[%]
F_v	=	cumulative bubble velocity distribution	[%]
H	=	column height	[m]
$k_l a$	=	volumetric liquid-phase mass transfer coefficient	[s^{-1}]
L_b	=	vertical bubble length (chord length)	[m]
$\bar{L}_b$	=	arithmetic mean of L_b in column	[m]
L_m	=	median of bubble length distribution	[m]
l	=	distance between two probes	[m]
n_b	=	bubble frequency	[s^{-1}]
$\bar{n}_b$	=	cross-sectionally averaged bubble frequency	[s^{-1}]
R_w	=	column radius	[m]
r	=	radial distance from axis	[m]
t	=	real time	[s]
U_b	=	bubble rising velocity	[m/s]
$\bar{U}_b$	=	arithmetic mean of U_b in column	[m/s]
U_g	=	superficial gas velocity	[m/s]
U_l	=	superficial liquid velocity	[m/s]
U_m	=	median of bubble velocity distribution	[m/s]
V_t	=	terminal settling velocity of a single particle	[m/s]
γ_l	=	surface tension of liquid	[N/m]
Δt	=	lag time between two probes	[s]
ε_g	=	gas holdup	[—]
$\bar{\varepsilon}_g$	=	cross-sectionally averaged gas holdup	[—]
ε_s	=	solid holdup	[—]

$\bar{\varepsilon}_s$	=	mean solid holdup	[—]
μ_l	=	liquid viscosity	[Pa·s]
ρ_l	=	liquid density	[kg/m^3]
σ_l	=	logarithmic standard deviation for bubble length distribution	[—]
σ_v	=	standard deviation for bubble velocity distribution	[m/s]
τ	=	bubble duration time at probe	[s]

Literature Cited

1) Akita, K. and F. Yoshida: *Ind. Eng. Chem., Process Des. Dev.*, **13**, 84 (1974).
2) Cova, D. R.: *Ind. Eng. Chem., Process Des. Dev.*, **5**, 20 (1966).
3) Deckwer, W.-D., Y. Louisi, A. Zaidi and M. Ralek: *Ind. Eng. Chem., Process Des. Dev.*, **19**, 699 (1980).
4) Hills, J. H.: *Trans. Inst. Chem. Engrs.*, **52**, 1 (1974).
5) Iida, Y.: *Nihon Genshiryoku Gakkaishi*, **14**, 13 (1972).
6) Kara, S., B. G. Kelkar, Y. T. Shah and N. L. Carr: *Ind. Eng. Chem., Process Des. Dev.*, **21**, 584 (1982).
7) Kato, Y.: *Kagaku Kōgaku*, **27**, 7 (1963).
8) Kato, Y., A. Nishiwaki, T. Fukuda and S. Tanaka: *J. Chem. Eng. Japan*, **5**, 112 (1972).
9) Kato, Y., A. Nishiwaki, T. Kago, T. Fukuda and S. Tanaka: *Kagaku Kōgaku*, **36**, 1333 (1972).
10) Kato, Y., M. Nishinaka and S. Morooka: *Kagaku Kogaku Ronbunshu*, **1**, 530 (1975).
11) Koide, K., A. Takazawa, M. Kōmura and H. Matsunaga: *J. Chem. Eng. Japan*, **17**, 459 (1984).
12) Kojima, H. and K. Asano: *Kagaku Kogaku Ronbunshu*, **6**, 46 (1980).
13) Matsuura, A. and L.-S. Fan: *AIChE J.*, **30**, 894 (1984).
14) Morooka, S., K. Uchida and Y. Kato: *J. Chem. Eng. Japan*, **15**, 29 (1982).
15) Neal, L. G. and S. G. Bankoff: *AIChE J.*, **9**, 490 (1963).
16) Rigby, G. R., G. P. Van Blockland, W. H. Park and C. E. Capes: *Chem. Eng. Sci.*, **25**, 1729 (1970).
17) Smith, D. N. and J. A. Ruether: *Chem. Eng. Sci.*, **40**, 741 (1985).
18) Suganuma, T. and T. Yamanishi: *Kagaku Kōgaku*, **30**, 1136 (1966).
19) Ueyama, K. and T. Miyauchi: *Kagaku Kogaku Ronbunshu*, **3**, 19 (1977).
20) Ueyama, K. and T. Miyauchi: *AIChE J.*, **25**, 258 (1979).
21) Ueyama, K., S. Morooka, K. Koide, H. Kaji and T. Miyauchi: *Ind. Eng. Chem., Process Des. Dev.*, **19**, 592 (1980).
22) Yamashita, F., Y. Mori and S. Fujita: *J. Chem. Eng. Japan*, **12**, 5 (1979).
23) Yasunishi, A., M. Fukuma and K. Muroyama: *Kagaku Kogaku Ronbunshu*, **12**, 420 (1986).

FLOW STRUCTURE AND MASS TRANSFER FOR A WAVY CHANNEL IN TRANSITIONAL FLOW REGIME

TATSUO NISHIMURA, YOSHIHIKO KAJIMOTO, ATSUSHI TARUMOTO AND YUJI KAWAMURA

Department of Chemical Engineering, Hiroshima University, Higashi-Hiroshima 724

Key Words: Fluid Flow, Vortex Structure, Transitional Flow, Wavy Channel, Mass Transfer, Flow Visualization, Electrochemical Method

The relationship between flow structure and mass transfer in a wavy channel was investigated in the range from laminar to turbulent flow. Laminar flow has a steady two-dimensional structure, but turbulent flow has an unsteady three-dimensional vortical structure. In particular, the flow field in a large recirculation vortex within the furrow of a wavy wall shows an intermittent reversed flow and a nonuniformity of flow in the spanwise direction for turbulent flow. The flow intermittency is closely related to the mass transfer, and a remarkable increment of mass transfer rate is induced near the flow reattachment point in the large recirculation vortex, which suggests a renewal of the concentration boundary layer because of the flow intermittency.

Introduction

The channel with wavy walls is one of several devices employed for enhancing the heat and mass transfer efficiency of processes having high Peclet numbers, such as in plate heat exchangers, electrodialyzers and membrane blood oxygenators.

In previous reports, heat and mass transfer for laminar flow has been analyzed by calculation,[1,3,4,5,7,8,10,15] while studies of fully turbulent flow have been carried out by experiment.[6,16-18] However, investigations in the transitional flow regime have been quite limited. Recently the authors[14,15] experimentally found that the increment of

Received March 5, 1986. Correspondence concerning this article should be addressed to T. Nishimura. Y. Kajimoto is now with Tokuyama Soda Co., Ltd., Tokuyama 745.